technical transactions

No. 2025/003

mechanics

sciendo

Torsional mode shapes of FGM shafts with various cross section

Mateusz Kumor

mateusz.kumor@doktorant.pk.edu.pl | https://orcid.org/0009-0009-4063-6584

Cracow University of Technology,
Faculty of Mechanical Engineering

Scientific Editor: Grzegorz Filo,
Cracow University of Technology
Technical Editor: Aleksandra Urzędowska,
Cracow University of Technology Press
Typesetting: Anna Pawlik,
Cracow University of Technology Press

Received: January 17, 2025
Accepted: April 25, 2025

Data Availability Statement: All relevant data are within the paper and its Supporting Information files.

Competing interests: The authors have declared that no competing interests exist.

Citation: Kumor, M. (2025). Torsional mode shapes of FGM shafts with various cross section. *Technical Transactions, e2025003*. https://doi.org/10.37705/TechTrans/e2025003

Abstract

In this study, the torsional mode shapes of circular and non-circular functionally graded material shafts, focusing on triangular, rectangular, circular cross--sections are investigated. The shafts are composed of an aluminum-titanium (AlTi) alloy and various functionally graded materials, utilizing different mixing rules to create a gradient surface. The modal analysis is conducted using ANSYS Mechanical leading finite element analysis software to assess and visualize the vibrational characteristics of these shafts under torsional loading. Then, the same shafts made of isotropic material (pure Al) is prepared, and compared with respect to results. The objective is to understand the influence of FGMs compared to homogeneous and isotropic materials on the torsional behavior of shafts with non-circular geometries. By comparing the torsional mode shapes and frequencies, one can identify the distinct vibrational properties introduced by the gradient material composition. This comparison is highlight the potential advantages of FGM shafts in applications requiring tailored mechanical properties that traditional homogeneous materials cannot provide. The study also explores how the different cross-sectional shapes affect the torsional response, which is crucial for designing components subjected to twisting loads in aerospace, automotive, and construction industries. The results from ANSYS Mechanical are analyzed to extract the mode shapes and frequencies of torsional modes, providing a comprehensive understanding of how FG materials behave relative to isotropic counterparts under similar conditions. The study aims to show how the natural frequency and torsional mode shapes differ for a functionally graded material compared to isotropic material, may be useful for researchers working with applications where vibration behavior is crucial.

Keywords: Torsional mode shapes; FGM; AlTi; Ansys; Natural frequency

1. Introduction

In recent years Functionally Graded Materials (FGM) interests have been increased. Manny articles regarding different mechanical states of FGM structures have been published. The works including states of tension, compression, bending and torsion of structures, beams, shafts etc. when analyzing publications concerning FGM structures, we can conclude that there are not many sources regarding twisting shape modes for beams and shafts. However, there are several sources describing the structure, plates, and beams of FGMs and their natural frequencies and mode shapes. Please allow me to present a few of them. The first of them are the works by Tabatabaei and Fattahi (2022), who performed a modal analysis of a rectangular cross-section beam made of FG material, and presented the mode shapes for different boundary conditions. Another work is by Murin et al. (2016), which describes the mode shapes for rectangular FGM beams that consider the effects of shear, transverse forces, and the Winkler's effect. In their subsequent works, Murin et al. (2014) published a solution for the modal analysis of a 3D beam with a doubly symmetric cross-section, also including the effects mentioned in their previous work. However, a solution for a wider range of cross-sections was not provided. Ashrafi et al. (2018) also described a modal analysis of FGM plates depending on different values of the parameter n, which comprises the content of pure materials as well as the FGM mixture in the entire composition. Huyen et al. (2017) have developed analysis of a functionally graded material (FGM) Timoshenko beam formulated in the frequency domain, accounting for the true neutral axis position, allowing for explicit expressions of the frequency equation, natural modes, and frequency response under external load. Khiem et al. (2023) have researched governing equations for free vibration of the cracked, functionally graded Timoshenko beam with a bonded piezoelectric layer and provides a general solution in the frequency domain. Khiem et al. (2020) in second work have investigated the Transfer Matrix Method (TMM) for analyzing free vibration of cracked continuous Timoshenko beams made of Functionally Graded Material (FGM), incorporating material grading, neutral plane position, and a double spring crack model. Mashat et al. (2014) have showed various structures, such as laminated beams with FG cores, thin- and thick-walled boxes, and sandwich cylinders, were analyzed, and the results in terms of natural frequencies were compared with those available in the literature. As it is commonly known, the shape modes obtained during modal analysis have a significant impact on the subsequent design of components in various industrial environments such as automotive, aerospace, and mining. Most commonly known analyses of this type refer to isotropic and homogeneous materials, and the study of the application of FGM materials is much less extensive. Many elements of the industry are subjected to numerous and various frequencies of mechanical vibrations originating from different sources. Depending on the frequencies of the natural vibrations of a given mechanical component, its resonant properties are evaluated. For different vibration frequencies, a given element is subjected to deformations caused by system vibrations. To avoid the phenomenon of resonance, structural elements subjected to installation vibrations are subjected to modal analysis. It is obvious that the reduction of natural vibration frequencies for isotropic and homogeneous materials occurs through increasing the mass of the element or manipulating its stiffness, which consequently involves altering the geometric dimensions of the given element. According to the frequency rule it is possible to obtain expression for natural frequency under torsion (see Timoshenko, 1983; Nayak and Armani, 2022).

$$\omega = \sqrt{k/m} \tag{1}$$

where ω is the natural frequency, k is the stiffness, and m is the mass of the system.

https://doi.org/10.37705/TechTrans/e2025003

Any system characterized by linearity and having a specific number of degrees of freedom n has ω_i natural frequencies of vibration, which are released after the system is displaced from its equilibrium. The natural frequencies of a structure are not dependent on the magnitude of the amplitudes. By formulating the differential equation of the vibrating motion of the body, after adopting the general equation of motion and considering the absence of external disturbances acting on the body or system, the following equation of motion is distinguished (see Kruszewski, 1975):

$$\boldsymbol{M}\ddot{\boldsymbol{x}}+\boldsymbol{C}\dot{\boldsymbol{x}}+\boldsymbol{K}\boldsymbol{x}=0 \tag{2}$$

where $\boldsymbol{x}$ is the displacement vector, $\dot{\boldsymbol{x}}$ is the first derivative of displacement, meaning the velocity, and $\ddot{\boldsymbol{x}}$ is the second derivative of displacement, meaning the acceleration, and $\boldsymbol{M}$, $\boldsymbol{C}$, $\boldsymbol{K}$ are a mass, damping and stiffness matrixes, respectively.

In the case of most structures, when calculating free vibrations, the effect of damping is negligible, which simplifies the equation of motion and the subsequent analysis of these structures. The equation without the damping term takes the following form (see Kruszewski, 1975; Gawroński et al., 1984):

$$\boldsymbol{M}\ddot{\boldsymbol{x}}+\boldsymbol{K}\boldsymbol{x}=0 \tag{3}$$

This equation can be reduced to a simpler matrix algebra form, which allows the results to be written in a more convenient way. After multiplying the mass matrix by $\boldsymbol{M}^{-1/2}$ the left side of the equation and applying the relevant transformations, we ultimately obtain the differential equation of motion for free vibrations in the form (see Kruszewski, 1975; Gawroński et al., 1984):

$$\ddot{\xi}+\boldsymbol{A}\xi=0 \tag{4}$$

where ξ and $\boldsymbol{A}$ is equal:

$$\xi=\boldsymbol{M}^{1/2}\boldsymbol{x} \tag{5}$$

$$\boldsymbol{A}=\boldsymbol{M}^{-1/2}\boldsymbol{K}\boldsymbol{M}^{-1/2} \tag{6}$$

In order to solve equation (4), it is necessary to introduce the harmonic form of this equation. The final version of the equation is as follows:

$$\xi=\xi^0\sin(\omega t+\psi) \tag{7}$$

$$\xi^0\left(\boldsymbol{A}-\boldsymbol{I}\omega^2\right)=0 \tag{8}$$

where $\boldsymbol{I}=\boldsymbol{M}^{-1/2}\boldsymbol{M}^{1/2}$ and ω is the angular frequency of vibrations of the n-degree.

In the context of functionally graded materials, the application of the above relationships reduces to making the stiffness matrix in the material dependent on the function of variation in relation to one of the directions of gradation. This results in the dependence of the interpolation of Gaussian integration at Gaussian points on the variable L, as shown by Kim and Paulino (see Kim and Paulino, 2002), in the case of natural vibrations, this reduces to making the stiffness matrix of each element dependent on the function of the changes in the material properties that form the gradient in the structure and in the specified direction. After substituting the dependencies, the equation of motion can be reduced to the following relationship:

$$\boldsymbol{M}\ddot{\boldsymbol{x}}+\boldsymbol{K}(L)\boldsymbol{x}=0 \tag{9}$$

Structural elements such as beams and shafts are relatively well-studied in terms of modal analysis, which can be achieved through numerical methods. When FGM structures are compared with isotropic structures, their resources are relatively scarce. The present article presents a numerical investigation using the commercial software Ansys, concerning the twisting shape modes for shafts with different cross-sections and comparing the results of resonant frequencies and twisting modes for FGM (AlTi) shafts and pure aluminum.

2. Governing material assumptions

The analysis involved three isotropic shafts made of pure aluminum and three shafts made of functionally graded material consisting of aluminum core and Titanium (AlTi). The shafts have various cross-sectional shapes including; circular, equilateral triangular, square. Each of the shafts has an equal cross--sectional area of $A = 7850\ \mathrm{mm}^2$ and a length of $l = 500\ \mathrm{mm}$. The load on each of the tested elements was applied kinematically. Shear modulus G for isotropic material has been calculated by use of formula (see Timoshenko, 1983)

$$G = E/2(1+\nu) \tag{10}$$

where E is a Young's modulus, ν is Poisson ratio.

All material properties are presented in temperature of 20°C and for isotropic material the linear Hooke's material model has been taken into account. The properties of isotropic shafts are presented in Table 1.

Table 1. Material properties for all isotropic shafts made of aluminum alloy

Cross section	Modulus of elasticity E [GPa]	Poisson ratio ν [–]	Density ρ [kg/m³]	Shear modulus G [GPa]
All sections	72	0.33	2699	27

The material properties of Young's modulus used for the graded shafts were derived based on mixture formula (see Aminbaghai et al., 2017)

$$E(y) = E_f + (E_m - E_f)(y/l)^n \tag{11}$$

where E_f is a Young's modulus of aluminum and E_m is a Young's modulus of titanium and $n = 1, 2, \ldots, 5$ is a number of graded layers power of polynomial.

A similar formula can be written to describe the changes in the Poisson's ratio with respect to the distance from the center of cross section y. The formula is as follows (see Aminbaghai et al., 2017)

$$\nu(y) = \nu_f + (\nu_m - \nu_f)(y/l)^n \tag{12}$$

Considering the above formulas, we can assume that the shear modulus for non-uniform torsion is equal to (see Aminbaghai et al., 2017)

$$G(y) = E(y)/2(1+\nu) \tag{13}$$

Thus, the formula for the mixing density is as follows (see Aminbaghai et al., 2017)

$$\rho(y) = \rho_f + (\rho_m - \rho_f)(y/l)^n \tag{14}$$

Instead of applying a division in the longitudinal direction, the properties of the gradient materials were approximated using the above formulas in the direction of changes with respect to the distance y from the center of the cross-

-section. The assumptions concerning the changes in material properties relate to changes in one direction x. Each of the examined cross-sections of the shafts was divided into equal distances in the direction of x and then approximated in terms of graded properties, in the middle of the cross section it's pure aluminum properties, the is changing gradually to pure titanium, see example Fig. 1. The material properties, such as Young's modulus, Kirchhoff's modulus and Poisson's ratio were derived using the above rule and are presented in the Table 2.

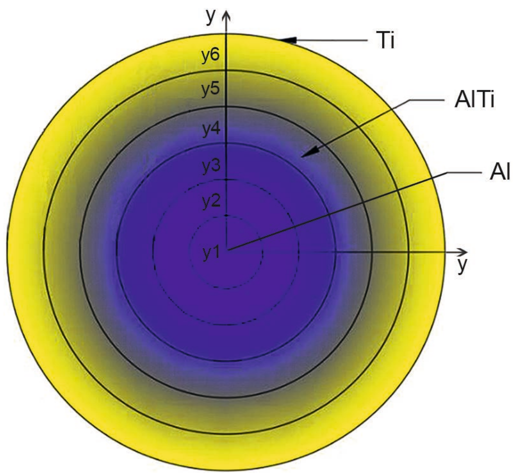

Fig. 1. Example of distribution of graded area in y direction

The Table 2 below presents the assumed material properties for the alloys of the individual materials from which the gradient was created according to the above rule.

Table 2. Material properties of aluminum and titanium alloy

Material property		
Young's modulus [GPa]	$E_f = 72$	$E_m = 116$
Kirchhoff's modulus [GPa]	$G_f = 27$	$G_m = 43.3$
Poisson's ratio [–]	$\nu_f = 0.33$	$\nu_m = 0.34$
Density [kg/m³]	$\rho_f = 2699$	$\rho_m = 4540$

Each of the tested shafts was divided into six graded layers x, for which values were approximated according to a mixing rule. The ratio of y/l for each section was equal, so for each of the shafts the graded properties depending on the length of the layer in the y direction will be identical. Below, in Table 4, the thicknesses of individual layers for individual cross-sections are presented, along with the graded properties, which were identical. In Figs. 2–4 the results of E, G and ν in function of distance y and exponent n in circular graded shaft have been presented. The above procedure was performed for all geometries,

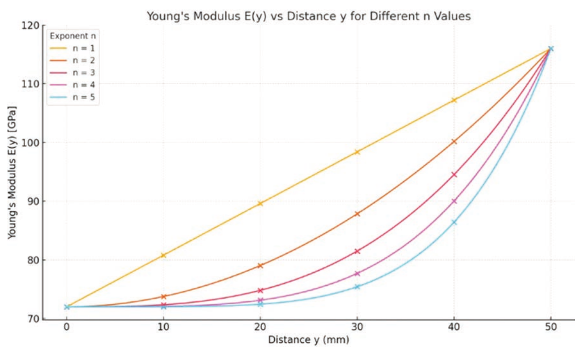

Fig. 2. Example of representation of E in function of distance y exponent n in graded round shaft

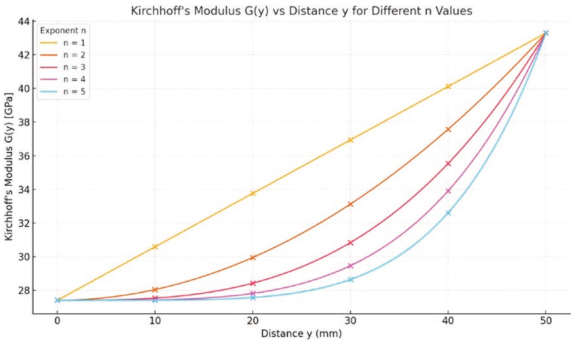

Fig. 3. Example of representation of G in function of distance y exponent n in graded round shaft

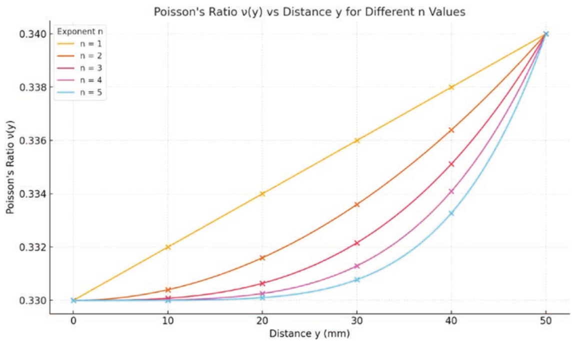

Fig. 4. Example of representation of ν in function of distance y exponent n in graded round shaft

Fig. 5. Example of representation of p in function of distance y exponent n in graded round shaft

however for reasons of transparency and a similar distribution of results, only the results for the example of a round shaft are shown.

The above plots present the material properties for various changes in the gradation distance y with respect to the circular cross-section over a distance $L = 50$ mm. As the exponent n increases, we observe a smoother transition between the graded phases within the cross-section. The ratio y/l in each of the cross-sections is identical, as is the number of layers. Therefore, in each case, the distribution of material properties as a function of n and distance y will be identical. All results have been presented in Table 3.

Table 3. Results of material graded properties dependent on exponent n

Property	n	Layer 1	Layer 2	Layer 3	Layer 4	Layer 5	Layer 6
E [GPa]	1	72	80.8	89.6	98.4	107.2	116
ν [–]	1	0.33	0.332	0.334	0.336	0.228	0.34
G [GPa]	1	27.06	30.33	33.35	36.826	40.06	43.3
ρ [kg/m^3]	1	2699	3067.2	3435.4	3803.6	4171.8	4540
E [GPa]	2	72	73.76	79.04	87.84	100.16	116
ν [–]	2	0.33	0.33	0.332	0.334	0.336	0.34

https://doi.org/10.37705/TechTrans/e2025003

G [GPa]	2	27.06	27.72	29.679	32.93	37.474	43.28
ρ [kg/m³]	2	2699	2772.64	2993.56	3361.76	3877.24	4540
E [GPa]	3	72	72.35	74.81	81.50	94.528	116
ν [–]	3	0.33	0.33	0.331	0.332	0.335	0.34
G [GPa]	3	27.068	27.19	28.113	30.591	35.401	43.28
ρ [kg/m³]	3	2699	2713.72	2816.82	3096.65	3641.592	4540
E [GPa]	4	72	72.07	73.126	77.702	90.022	116
ν [–]	4	0.33	0.33	0.33	0.331	0.334	0.34
G [GPa]	4	27.06	27.094	27.486	29.183	33.739	43.28
ρ [kg/m³]	4	2699	2701.94	2746.13	2937.59	3453.07	4540
E [GPa]	5	72	72.014	72.451	75.42	86.418	116
ν [–]	5	0.33	0.33	0.33	0.331	0.333	0.34
G [GPa]	5	27.06	27.073	27.23	28.337	32.408	43.28
ρ [kg/m³]	5	2699	2699.58	2717.85	2843.15	3302.25	4540

The torsion shape modes will be extracted for exponents n from 1 to 5 and compared with the modes for aluminum isotropic material.

3. Geometry representation

The geometry for the tested shafts was created in Space Claim and then opened in the Ansys Workbench modal module. The analysis focused on the mode shapes and natural frequencies for each shaft. The results are divided into two cases: shafts with isotropic approximated FGM layers and shafts with homogeneous isotropic material (aluminum). Below, simplified schematics of FGM shafts geometry are presented in the Figs. 6–8.

Each of the shafts was prepared as 3D shafts. Additionally, shafts made of FGM material were divided into layers of equal thickness in relation to one of the directions of the cross-section according to the mixing rule. The first layer L1, positioned closest to the center of each section, was made of one hundred percent aluminum, while the subsequent layers contained respective amounts of a mixture of aluminum and titanium. The outermost layer is titanium with its pure properties. The isotropic geometries were made entirely of aluminum. The dimensions of each geometry were selected in such a way that they all presented identical surface areas equal to about 7850 mm².

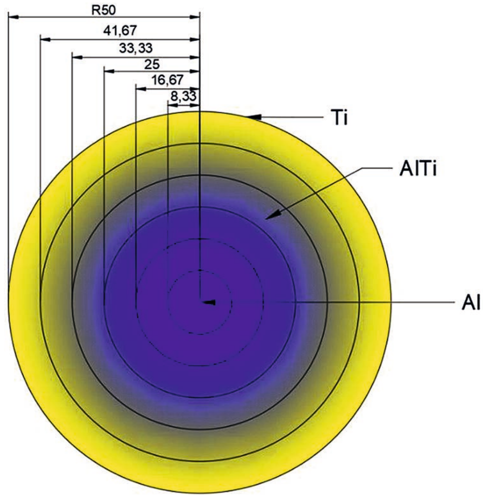

Fig. 6. Geometry of layered FGM rounded shaft composed with Al core

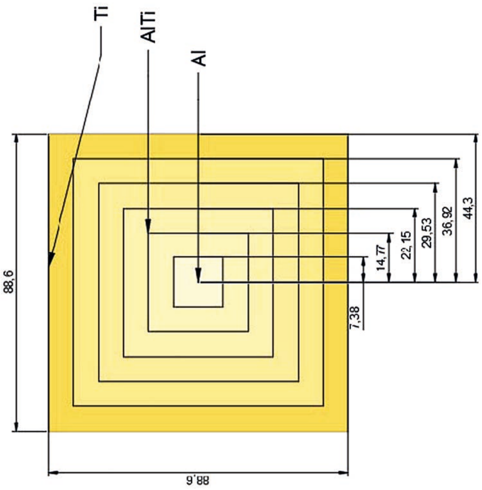

Fig. 7. Geometry of layered FGM square shaft composed with Al core

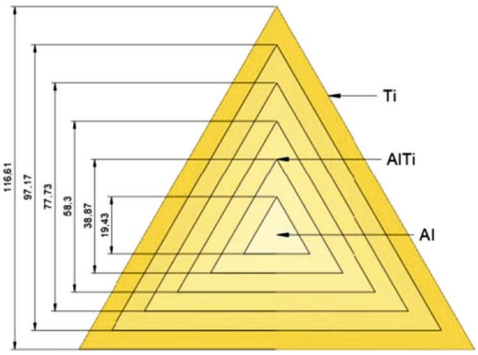

Fig. 8. Geometry of layered FGM triangle shaft composed with Al core

4. Torsional mode shape and natural frequency results

For all the shafts, a finite element mesh was applied using the sweep function – a hexagonal mesh with a finite element size of 3.8 mm for cycle shaft 6.4 for square shafts and 6.2 for triangular. The quality of the mesh was determined based on the Jacobian parameters, Aspect Ratio, and Element Quality. All these parameters indicated very favorable values. Using the Remote Displacement function, all degrees of freedom were constrained at one end of each shaft, and then a Fixed type modal analysis was conducted. Twelve modes of shape were requested for each analysis, and then only the torsional modes and their corresponding natural frequencies were recorded and documented. First, the cases of shafts made from isotropic and homogeneous material, aluminum, were analyzed, and then a modal analysis was conducted for shafts with assigned layers of materials simulating a gradient of properties. The obtained results of the mode shapes and natural frequencies for each of the shafts are presented in the following Figs 9–26.

Figures 9–26 presented illustrate the torsional mode shapes for all shaft examples. A comparison of the results will be discussed in Chapter 5.

https://doi.org/10.37705/TechTrans/e2025003

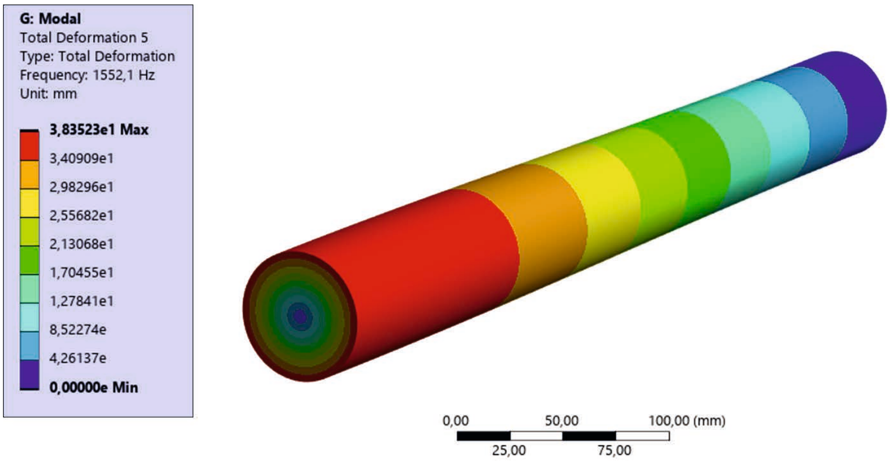

Fig. 9. Torsional mode and natural frequency of round isotropic Al shaft

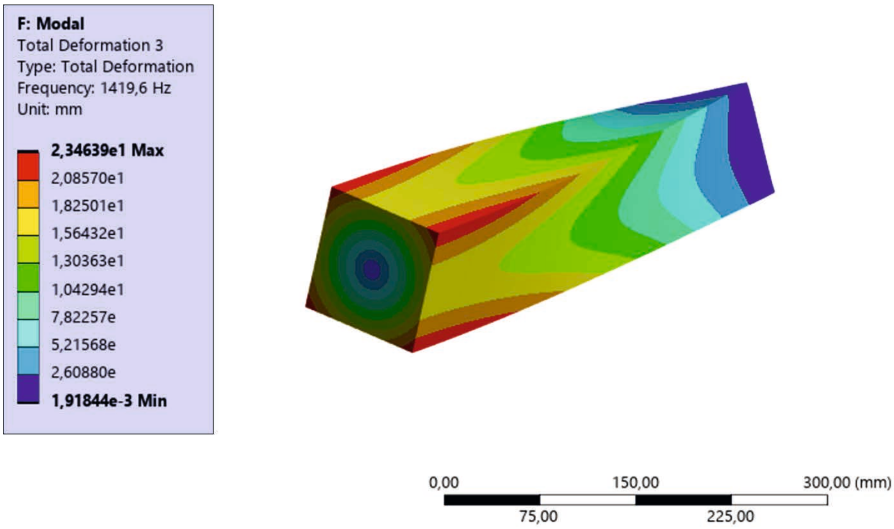

Fig. 10. Torsional mode and natural frequency of square isotropic Al shaft

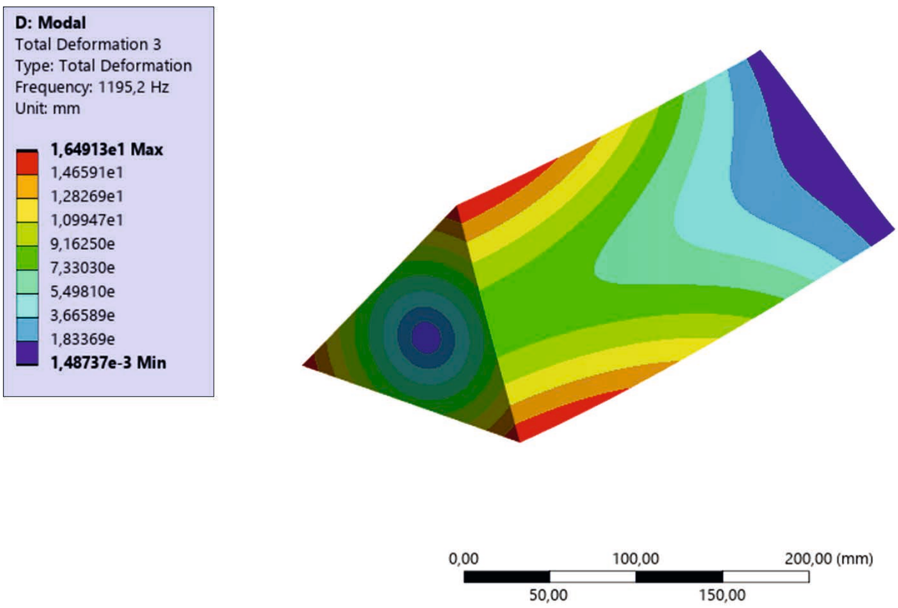

Fig. 11. Torsional mode and Natural frequency of triangle isotropic Al shaft

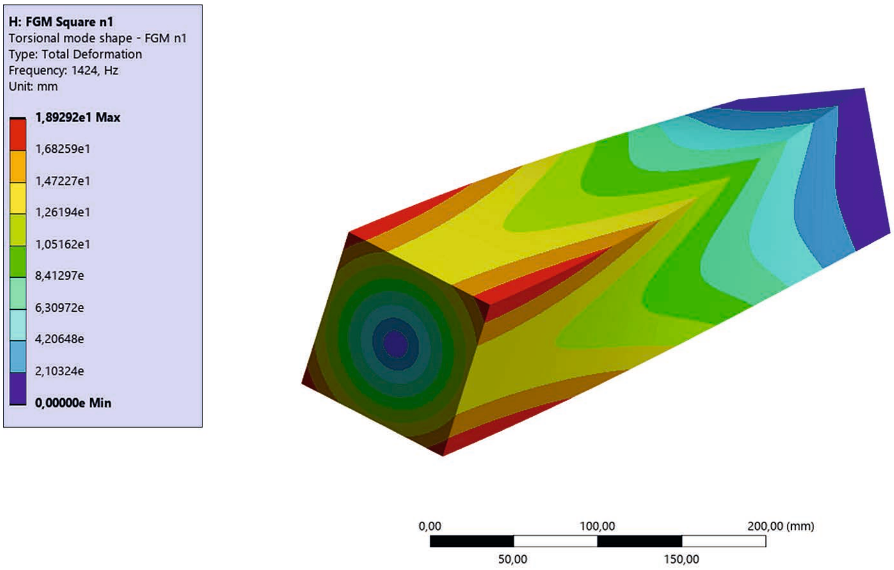

Fig. 12. Torsional mode and natural frequency of square FGM shaft with polygonal $n = 1$

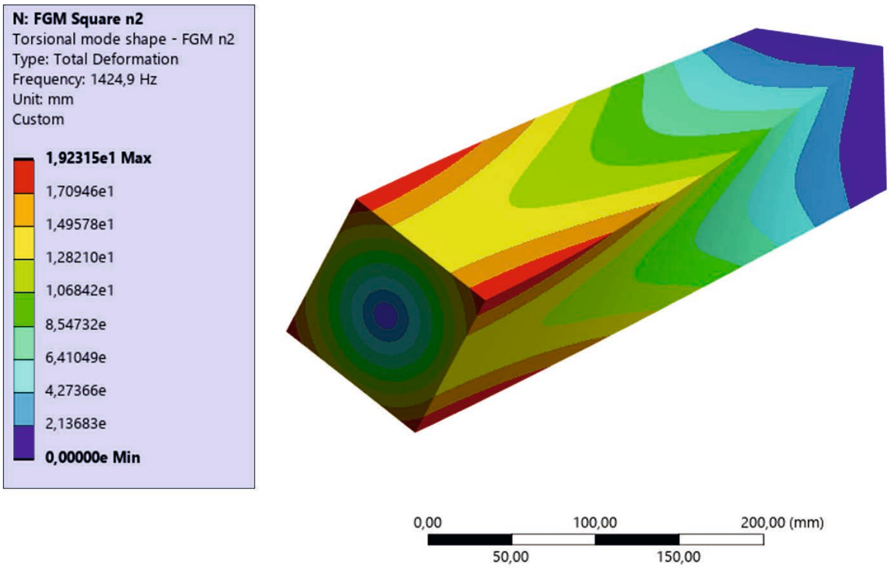

Fig. 13. Torsional mode and natural frequency of square FGM shaft with polygonal $n = 2$

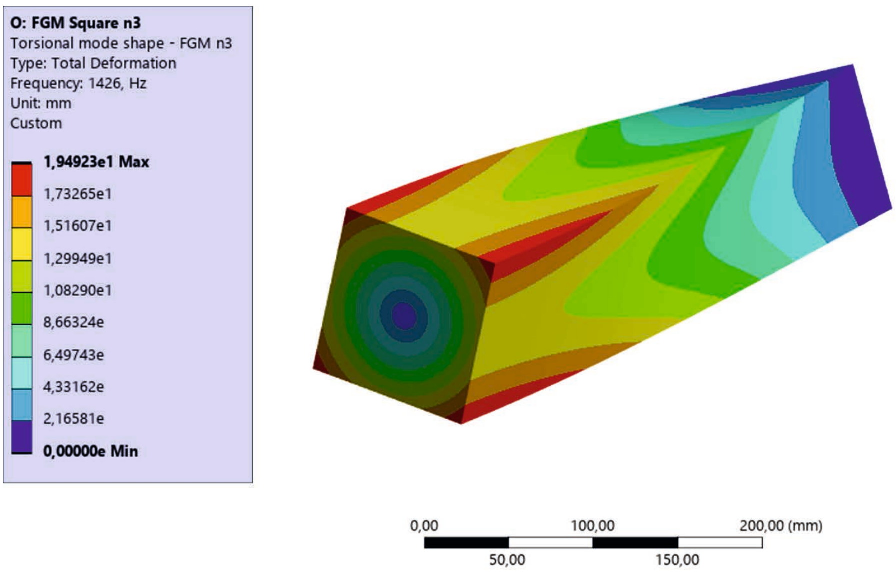

Fig. 14. Torsional mode and natural frequency of square FGM shaft with polygonal $n = 3$

https://doi.org/10.37705/TechTrans/e2025003

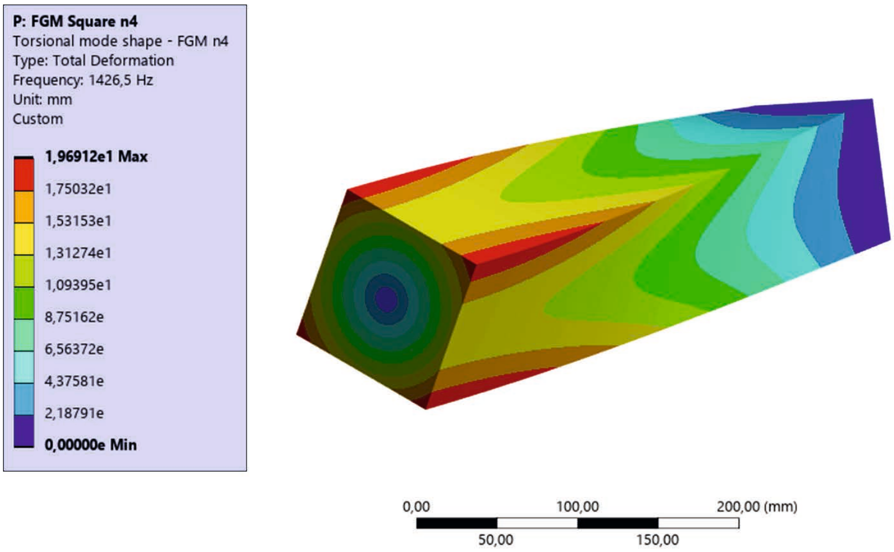

Fig. 15. Torsional mode and natural frequency of square FGM shaft with polygonal $n = 4$

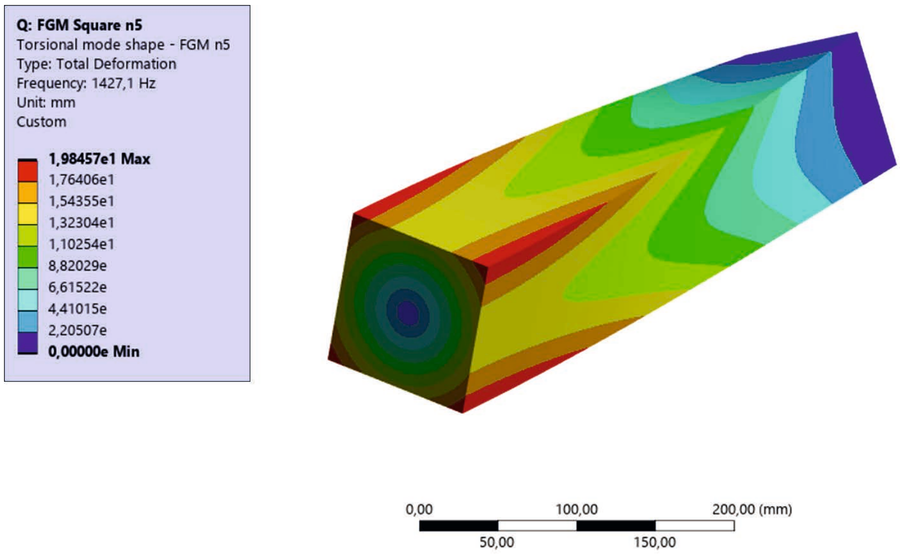

Fig. 16. Torsional mode and natural frequency of square FGM shaft with polygonal $n = 5$

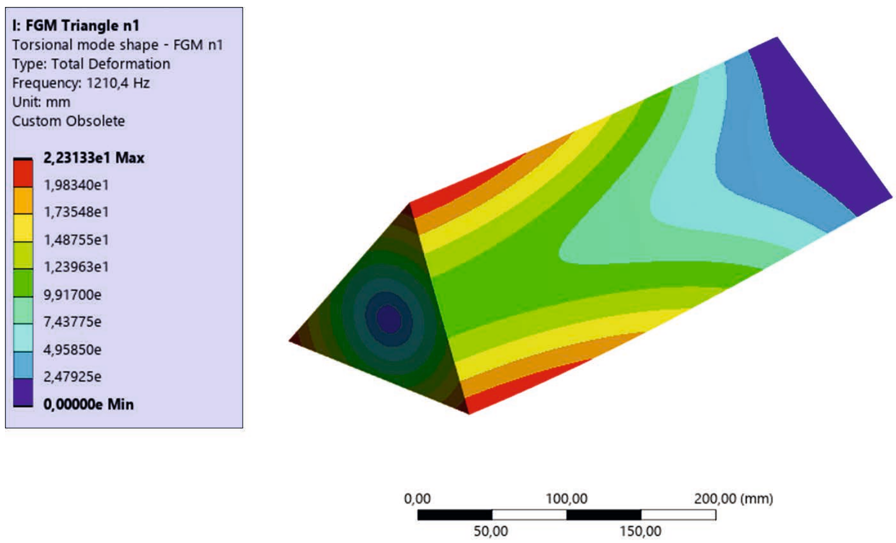

Fig. 17. Torsional mode and natural frequency of triangle FGM shaft with polygonal $n = 1$

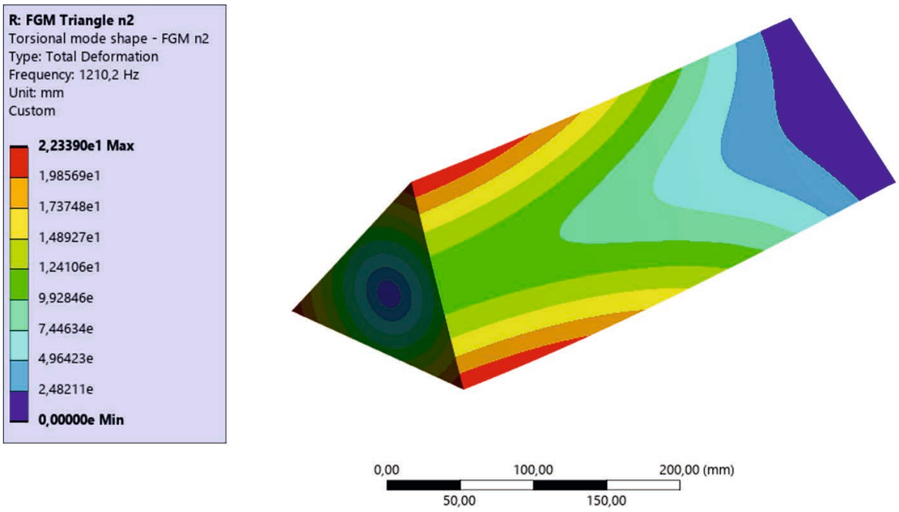

Fig. 18. Torsional mode and natural frequency of triangle FGM shaft with polygonal $n = 2$

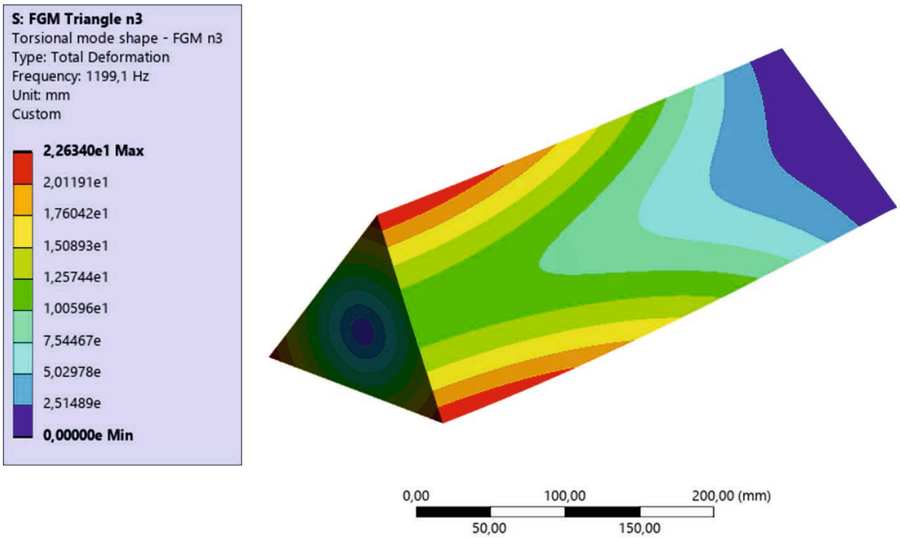

Fig. 19. Torsional mode and natural frequency of triangle FGM shaft with polygonal $n = 3$

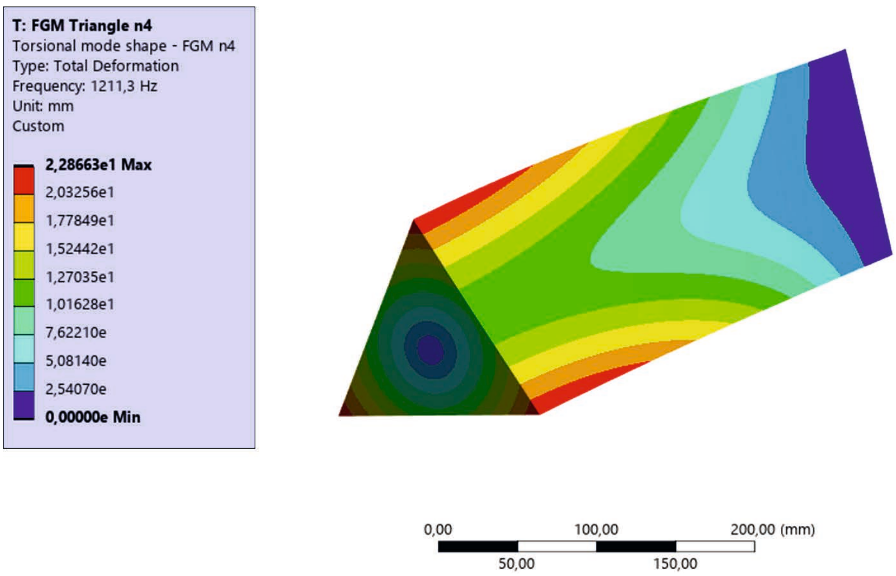

Fig. 20. Torsional mode and natural frequency of triangle FGM shaft with polygonal $n = 4$

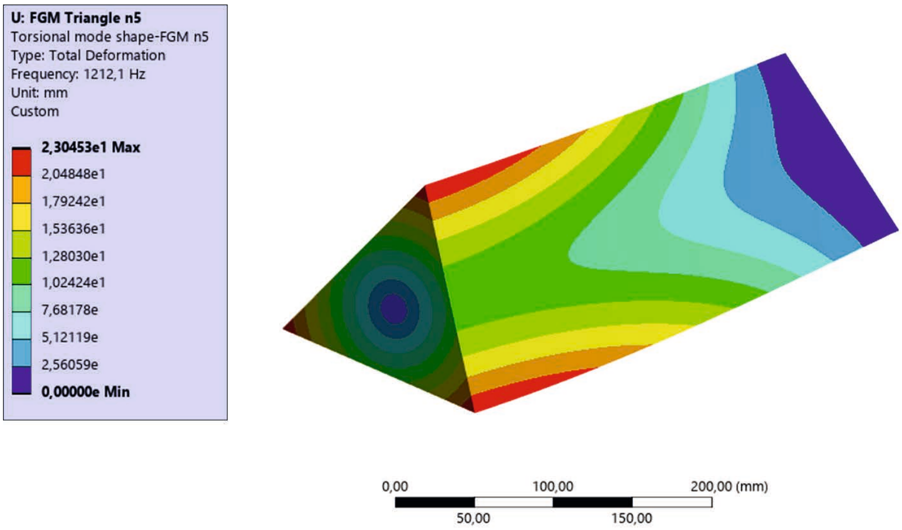

Fig. 21. Torsional mode and natural frequency of triangle FGM shaft with polygonal $n = 5$

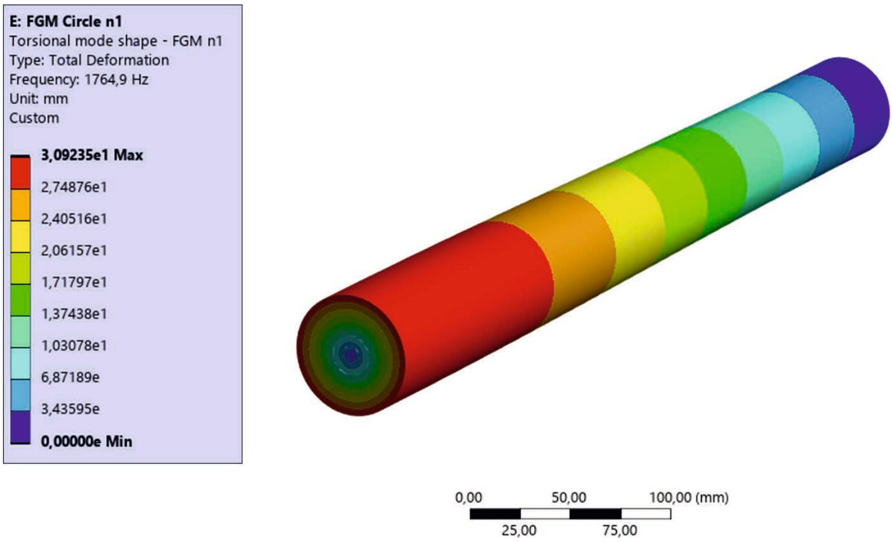

Fig. 22. Torsional mode and natural frequency of circle FGM shaft with polygonal $n = 1$

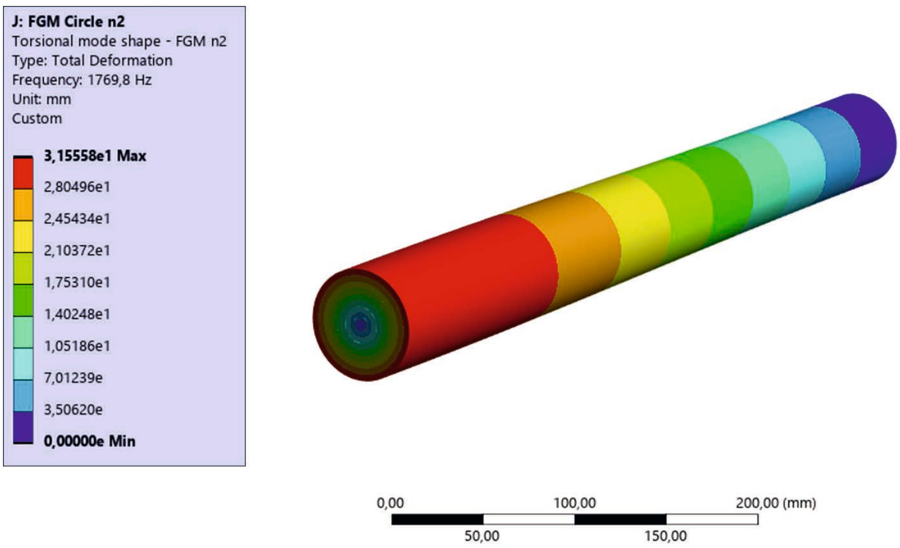

Fig. 23. Torsional mode and natural frequency of circle FGM shaft with polygonal $n = 2$

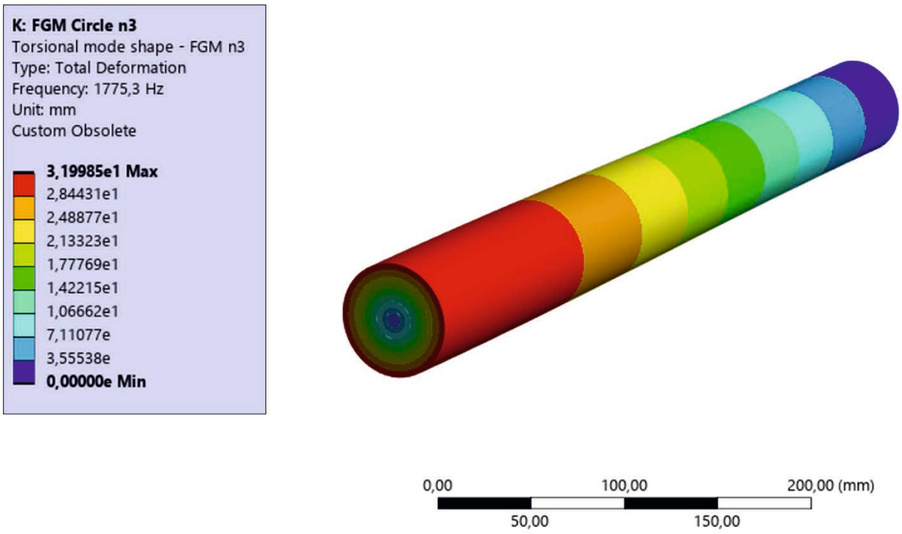

Fig. 24. Torsional mode and natural frequency of circle FGM shaft with polygonal $n = 3$

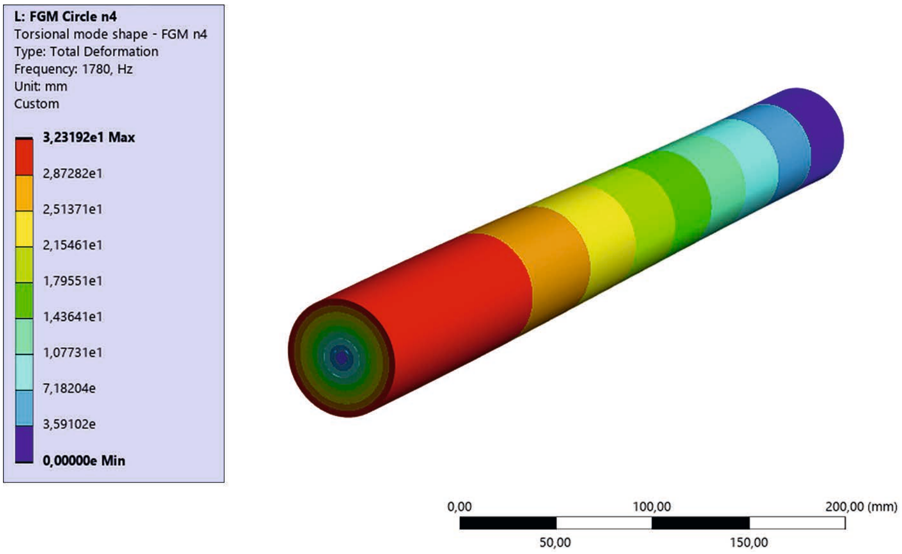

Fig. 25. Torsional mode and natural frequency of circle FGM shaft with polygonal $n = 4$

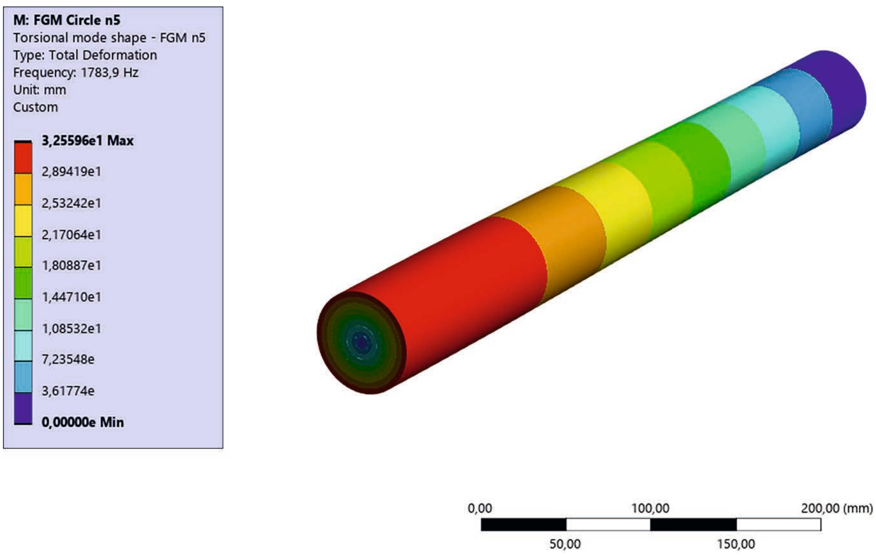

Fig. 26. Torsional mode and natural frequency of circle FGM shaft with polygonal $n = 5$

5. Comparison of isotropic and FGM results

Analyzing the mode shapes and natural frequencies reveals numerous differences between the shafts. The results are categorized into shafts with FGM cores and isotropic aluminum shafts. Below is a detailed discussion based on the results presented in Tables 4 and 5.

Table 4. Torsional mode results for cross-sections with aluminum

Cross section Al	Natural frequency [Hz]	Torsional mode shape [mm]	Participation factor [–]	Effective mass [–]	Effective mass to total mass [–]
Circular	1552.1	38.352	0.829	0.688	0.81
Squere	1419.6	23.467	–3.398	11.497	0.808
Triangle	1185.4	27.763	–3.437	11.816	0.79

Understanding the highest values of natural frequency of isotropic cross--sections related to the torsional shape modulus shows that shafts with cross--sections similar to circular ones exhibit them. The further the cross-section shape deviates from circular, the lower the natural frequency of vibrations, being minimal for a triangular shaft. It is therefore a quite understandable fact, as shafts with shapes close to circular possess rotational symmetry, resulting in a uniform distribution of mass and torsional stiffness, which ultimately leads to higher natural frequencies of their vibrations. As can be observed, the mode participation factor for isotropic sections of rectangular and triangular shapes takes negative values. This is related to the movement of the mass in relation to the direction of the applied excitation force, which are shifted by 180° relative to each other. The negative mode participation factor in these sections may be related to their asymmetry with respect to the axis of rotation and, consequently, the asymmetry in which the distributions of mass and stiffness are uneven, ultimately causing parts of the mass to move in the opposite direction to the applied load. Another contributing factor is, of course, the different mode shapes, which can have varying values of vibration in different parts of the section. The ratio of effective mass to total mass indicates the amount of mass transferred during a given mode shape. Therefore, if the values are close to 1, that mode gains more significance. For each of the shapes, for the identified 12 mode shapes.

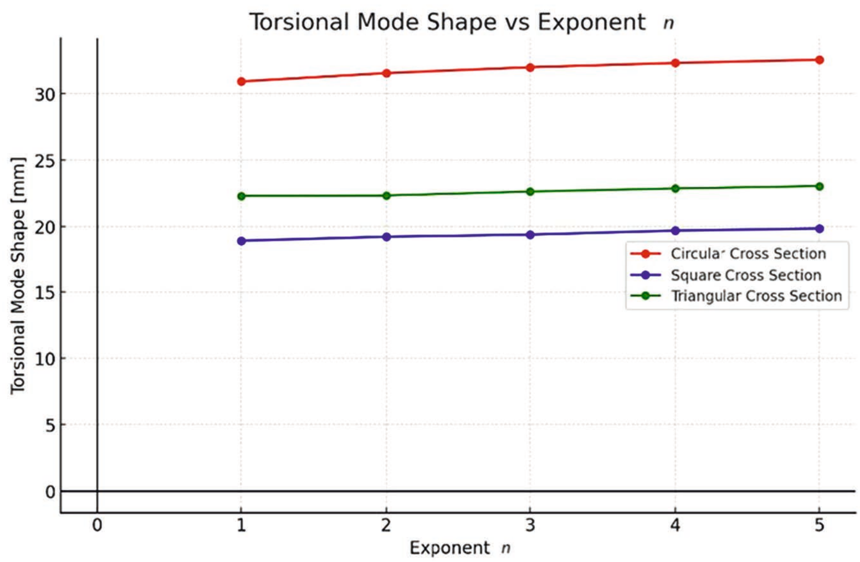

Fig. 27. Torsional mode in exponent n function

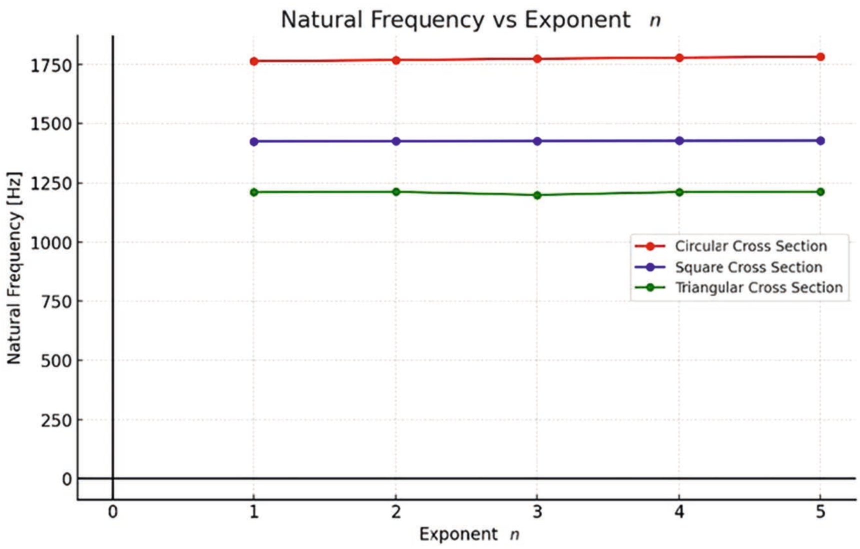

Fig. 28. Natural frequencies shape in exponent n function

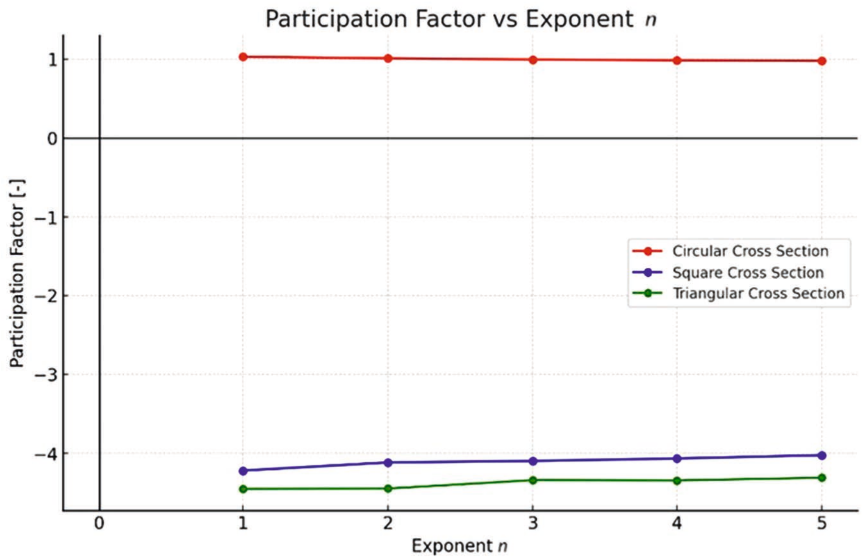

Fig. 29. Participation factor in exponent n function

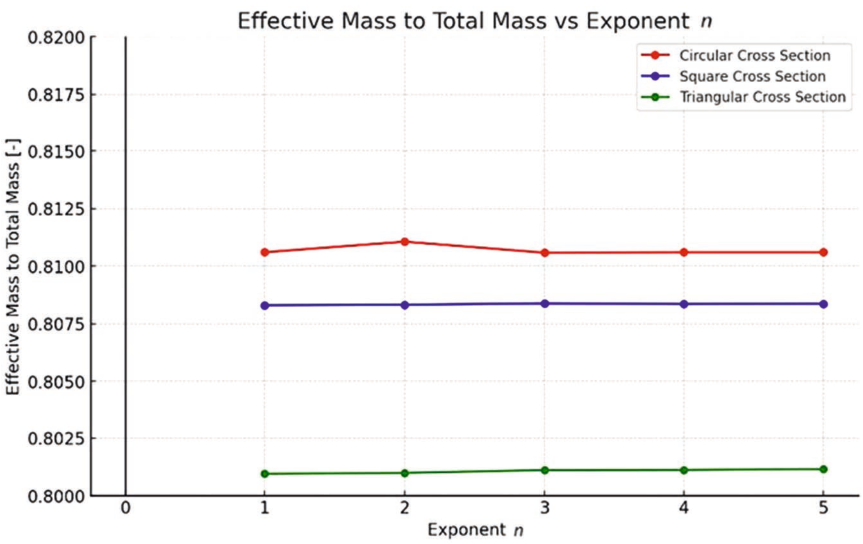

Fig. 30. Effective mass to total mass in exponent n function

https://doi.org/10.37705/TechTrans/e2025003

Observing the results of the natural frequencies, it can be noted that the exponent n affects the natural frequency of vibration of FGM shafts. The trend shows an increase in natural frequency with an increase in the exponent n for each FGM geometry. A similar situation occurs for the torsional mode shape deformations, where the trend for each cross-sectional shape also shows an increase in deformations with an increase in the exponent n. The effective mass to total mass ratio is also dependent on the exponent n and the cross--sectional shape. The highest values are observed for the circular FGM cross--section, while the lowest are for the triangular cross-section. The participation factor for the FGM sections shows positive values only for the circular cross--section, decreasing with respect to the exponent n; for the other sections, it takes negative values and increases with respect to n. The values of natural frequencies and mode shapes for shafts made of FGM material present differently. The values of the mode shapes also changed, each of the cross--sections showed a reduction in maximum deformation for the torsion mode, where the highest percentage was for a circular shaft.

Table 5. Torsional mode results for cross-sections with FGM

Cross-section FGM	Natural frequency [Hz]	Torsional mode shape [mm]	Participation factor [–]	Effective mass [–]	Effective mass to total mass [–]
Circular nr 1	1764.9	30.924	1.0294	1.05971	0.8106
Square nr 1	1424	18.929	–4.2179	17.7906	0.8832
Triangular nr 1	1210.8	22.313	–4.4505	19.8066	0.8094
Circular nr2	1769.8	31.556	1.0088	1.01766	0.8110
Square nr 2	1424.9	19.231	–4.1515	17.2351	0.8083
Triangular nr 2	1210.2	22.339	–4.4452	19.7599	0.8009
Circular nr 3	1775.3	31.998	0.994	0.989	0.8105
Square nr 3	1426	19.492	–4.0959	16.7763	0.8983
Triangular nr 3	1199.1	22.634	–4.3386	19.2443	0.8011
Circular nr 4	1780	32.319	0.984	0.97	0.8105
Square nr 4	1426.5	19.691	–4.0545	16.4388	0.8083
Triangular nr 4	1211.3	22.866	–4.3424	18.8566	0.8011
Circular nr 5	1783.9	32.56	0.977	0.955	0.8105
Square nr 5	1427.1	19.846	–4.0229	16.1835	0.8083
Triangular nr 5	1212.1	23.045	–4.3086	18.5643	0.8011

The use of two materials with significant density differences (aluminum and titanium) results in an increase in the mass of each of the shafts made from FGM material. This also affects the behavior under the influence of torsional vibrations, as the greater mass leads to a reduction in the frequency of vibrations. The increase in modal participation factor leads to an increase in the effective mass for FGM shafts, which directly affects its distribution in the structure. The increase in mass factor can be associated with the use of layers with a gradational structure. Aluminum as an alloy itself has lower torsional stiffness values; however, when FGM layers combined with a titanium alloy, which has much higher torsional stiffness values, were extracted, a final gradient with mixed AlTi properties was created, resulting in increased material stiffness in each of the $L(x)$ layers. This provides higher torsional stiffness values than in the case of aluminum alone, which affects the mass factor during torsion modes, increasing its values for each of the FGM shafts.

The charts in Figs 31 and 32 present the relationships between the natural frequency and shape modes depending on the material used and the cross--sectional area of the given shaft. The highest natural frequency values were achieved by shafts with circular cross-sections, both for aluminum and FGM. Isotropic materials exhibited lower natural frequencies for each of the cross--sections. The lowest natural frequency values were presented by the triangular cross-sections. The validity and reliability of the vibration analysis are also confirmed by the high ratio of effective mass transferred by the torsional mode to the total mass of the tested shafts. Across the identified 12 shape modes, this ratio exceeded 80% for each of the tested objects, and for most cross--sections related to torsion along the z-axis.

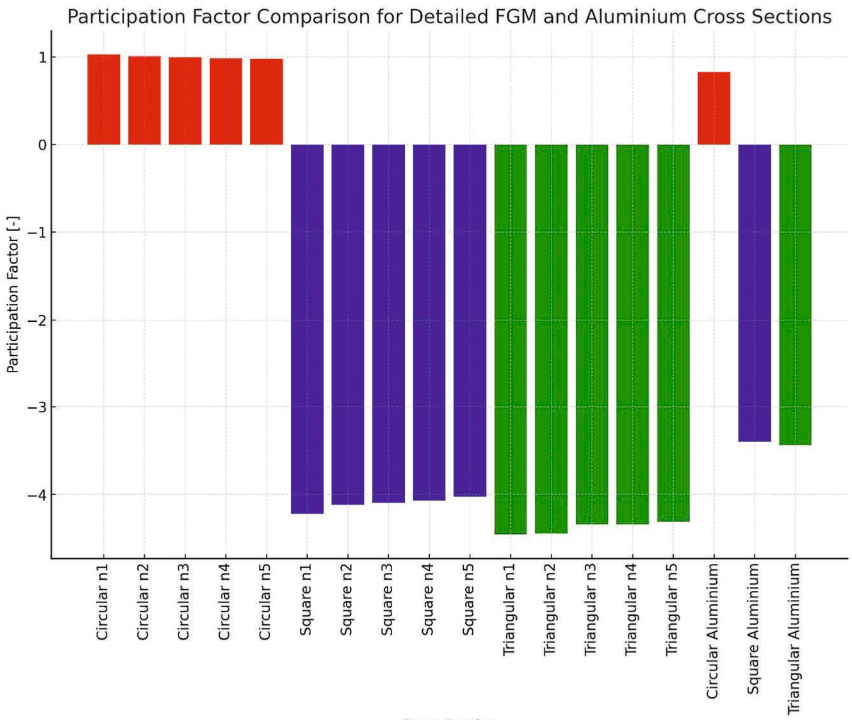

Fig. 31. Participation factor dependent on the cross-section and material

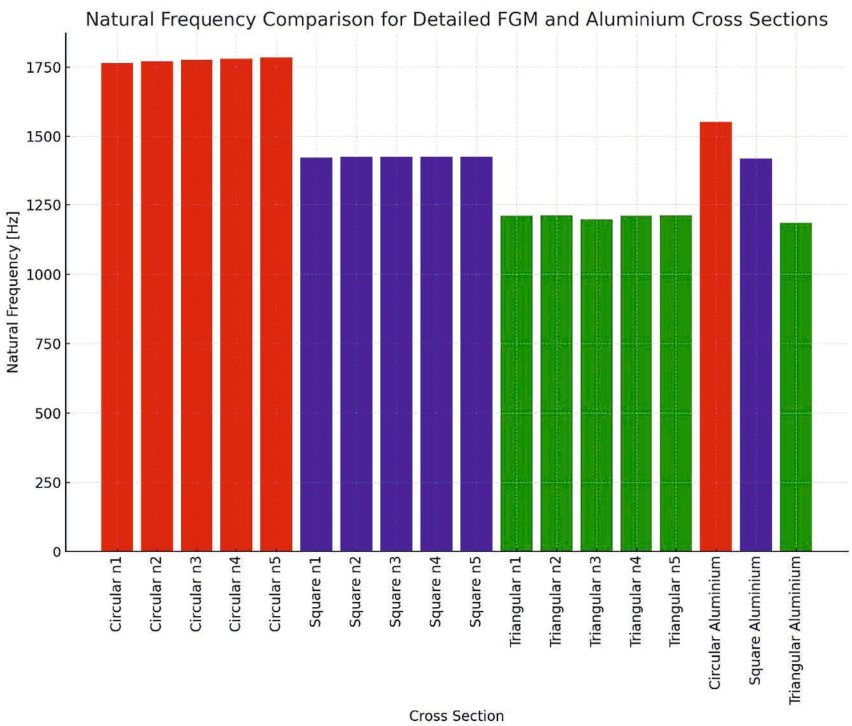

Fig. 32. Natural frequency dependent on the cross-section and material

6. Conclusions

The article presents a modal analysis of homogeneous and isotropic shafts (aluminum) and shafts made of FGM materials (AlTi) with homogeneous finite elements. The focus was on the shape modes and natural frequencies related to torsion. The obtained results were compared based on the analysis performed in Ansys software. This analysis was conducted for shafts with different cross--sectional areas. The following conclusions can be drawn from the presented results:

- the gradation and application of AlTi material in the structure of the shaft's cross-sections significantly affect the natural vibration frequencies of all the presented shafts,
- in each of the FGM cross-sections, a significant reduction in natural vibration frequencies was observed,
- the application of the FGM structure increases the indicators of participation factor and effective mass in each cross-section, indicating a greater influence of the FGM shafts on the torsional mode and its vibrational behavior,
- shapes close to circular have better natural vibration properties compared to non-circular geometries, both for aluminum and FGM materials,
- the application of FGM AlTi material for the torsional shape mode reduces natural vibrations, making shafts with FGM structure more suitable for applications with low-frequency vibration excitations,
- the lowest natural vibration frequencies were found in cross-sections of triangular,
- increasing the exponent in the material model causes an increase in the natural frequencies of all FGM shafts, as well as in the values of torsional mode shapes and participation factors.

Further investigations into the torsional modes of FGM structures may remain a compelling area of research, particularly when continuous gradation is taken into account. Analyzing torsional modes under such conditions may reveal notable differences. Additionally, experimental studies aimed at validating and confirming the FEM model could play a significant role in the continued advancement of functionally graded material dynamics.

References

Aminbaghai, M., Murín, J., Balduzzi, G., Hrabovsky, J., Hochreiner, G., Mang, H.A. (2017). Second-order torsional warping theory considering the secondary torsion moment deformation-effect. *Eng. Struct*. 147, 724–773.

Ashrafi, H.R., Beiranvand, P., Aghaei, M.Z., Jalili, D.D., (2018). Modal analysis of FGM plates (Sus304/Al2O3) using FEM. *Bioceram Dev Appl*, *8*(112), 2.

Gawroński, W., Kruszewski, J., Ostachowicz, W., Tarnowski, J., Wittbrodt E. (1984). *Finite element method in structural dynamics*. Warszawa: Arkady.

Huyen, Nguyen Ngoc, and Nguyen Tien Khiem (2017). Modal analysis of functionally graded Timoshenko beam. *Vietnam Journal of Mechanics 39*(1): 31–50.

Khiem, N.T., Hai, T.T., & Huong, L.Q. (2023). Modal analysis of cracked FGM beam with piezoelectric layer. *Mechanics Based Design of Structures and Machines 51*(9): 5120–5140.

Khiem, N.T., Tran, H.T., & Nam, D. (2020). Modal analysis of cracked continuous Timoshenko beam made of functionally graded material. *Mechanics Based Design of Structures and Machines 48*(4): 459–479.

Kim, J.-H., Paulino, G.H. (2002). Isoparametric graded finite elements for nonhomogeneous isotropic and orthotropic materials, *J. Appl. Mech. 69*(4): 502–514.

Kruszewski, J. (1975). *Finite stiff element method*. Warszawa: Arkady.
Mashat, Daoud, S., et al. (2014). Free vibration of FGM layered beams by various theories and finite elements. *Composites Part B: Engineering 59*: 269–278.
Murin, J., Aminbaghai, M., Hrabovsky, J., Kutis, V., Paulech, J., Kugler, S. (2014). A new 3D FGM beam finite element for modal analysis. In: Proceedings of the 11th world congress on computational mechanics (WCCM XI), 5th European conference on computational mechanics (ECCM V), 6th European conference on computational fluid dynamics (ECFD VI). Barcelona.
Murin, J., Aminbaghai, M., Hrabovsky, J., Gogola, R., Kugler, S. (2016). Beam finite element for modal analysis of FGM structures. *Engineering Structures 121*: 1–18.
Nayak, P., Armani, A. (2022): Optimal design of functionally graded parts. *Metals 12*(8), 1335.
Tabatabaei Shahidzadeh, S.J., Fattahi, A.M. (2022). A finite element method for modal analysis of FGM plates. *Mechanics Based Design of Structures and Machines 50*(4), 1111–1122.
Timoshenko, S. (1983). *History of strength of materials: with a brief account of the history of theory of elasticity and theory of structures*. Courier Corporation.